Heat Transfer Analysis and Estimation of CHF in Vertical Channel

K. Dolati Asl[1], E. Abedini[1*], Y. Bakhshan[1], A. Mohammadi Karachi[1], R. Hamidi Jahromi[1]

Abstract – Heat transfer occurs in flow boiling; as a result, the amount of heat between the tube wall surface and the fluid at different points of the tube may vary depending on the volume percent of vapor at those points. If the flow is fully vaporized, it does not allow for perfect heat transfer at that point; this significantly increases the temperature there; in this case the applied heat flux is called critical heat flux (CHF). The present paper has focused its attentions on simulating a two-phase fluid flow within the CHF range using ANSYS Fluent. The simulation results indicated an average error below 7%, which is more than those obtained by the experimental results. The maximum temperature of the tube surface when applying CHF could range between 200 and 500 K degrees more than that of fluid saturation according to the fluid working conditions. It also should be noted that both CHF and maximum temperature increase as the input pressure and mass flux do increase.

Keywords: Critical Heat Flux, Boiling, Two-phase flow, Simulation.

I. Introduction

The subcooled flow boiling occurs when the temperature of fluid is lower than the saturation temperature at a point but the wall temperature is so high that the boiling phenomenon will take place. Subcooled flow boiling has many applications in industries, such as heat transfer inside the core of nuclear reactors. It is possible to increase the heat disposal from the heated surface using subcooled flow boiling, but sometimes, when the excessive amount of applied heat flux on the wall can prevent the heat disposal, on the contrary, it causes the wall temperature increases too high which in turn may lead to damages of the surface. The heat flux value, which leads to a sharp rise in heated surface temperature is called critical heat flux. Practically, it is necessary to predict the critical heat flux value to prevent surface damage. In recent years, the heat flux value was investigated using the experiments, experimental and semi-experimental approaches. Many of the proposed correlations have good accuracy in estimating the heat flux value, but usually, they depend on the geometry, the working conditions, and the fluid type in usage, besides others. Researchers have to use different conditions in their experiments to obtain the critical heat flux value, which not only has high cost and time, but also is too complicate for calculation of some parameters such as temperature distribution in complex geometries. Progress in the field of subcooled flow boiling has made it easier to simulate and predict the critical heat flux value by the computer. Kim et al. studied CHF for fluid flow in a vertical tube using experimental method [1]. The experimental results showed that before reaching the CHF, the temperature of the tube wall would be 220 ° C and when the heat flux reaches CHF, the temperature of the tube is at 870 ° C with a sudden jump, which is very high and dangerous temperature for laboratory equipment. Chen et al. simulated the subcooled flow boiling of refrigerant-based fluid (R-113) inside the vertical tube using ANSYS CFX solver [2]. They studied the physical properties and bubble diameter. They found that boundary layer thickness increases as a function of increasing CHF value. Ose and Kunugi studied pool boiling phenomenon using computational fluid dynamics method [3]. Krepper *et al.* used RPI model for simulation and studied water and R-12 fluid flow in the heated vertical tube [4, 5, 6]. The RPI is an improved model to study the flow boiling [7]. Nasiri and Rashidi worked on subcooled flow boiling inside the two dimensional sinusoidal channel using computer simulation [8]. The results expressed that, variation of channel area as well as that of the pressure at different parts of the channel increase the vapor volume fraction value. Alimoradi *et al.* studied the subcooled flow boiling inside the channels with different cross sections [9]. Mohammadi and Khayat examined the effect of surface roughness on the bubble movement and CHF in pool boiling using experimental method [10]. The results showed that improvements in the

1* Corresponding Author : Department of Mechanical Engineering, University of Hormozgan, Bandar Abbas,, Iran.
Email: abedini@hormozgan.ac.ir, ehsan.abedini@gmail.com
2 Department of Mechanical Engineering, University of Hormozgan, Bandar Abbas,, Iran.
Received 2018.09.28 ; Accepted 2019.06.10

surface, increase the CHF and heat transfer coefficient values about 131 % and 211%, respectively. Many different correlations proposed for estimation of CHF in fluid flow. Wang et al. proposed correlation for calculation of CHF value [11]. They used the experimental results to provide their correlations. They have proposed correlation based on the tube diameter, inlet mass flux, and temperature and pressure. They have indicated that the proposed correlation is applicable for the pressure in the range of 400 to 890 *kPa* and the mass flux between 98.9 and 348.4 kg/m^{2}s. In the present research, simulation of water fluid flow inside the vertical tube has been done using RPI boiling model and using the results, the critical heat flux value would be estimated.

II. Mathematical modeling

During Two phases of water liquid and water vapor are used in flow boiling. The relationship between the two phases of liquid and vapor is investigated using Eulerian model. In this study, we have used the critical heat flux model based on the RPI boiling for the purpose of boiling simulation. The liquid and vapor phases are assumed to be continuous.

III. Governing equations for the Eulerian multiphase model

In order to simulate the present work, the Eulerian multiphase model has been used. The associated governing and auxiliary relationships for the selected model are:

A. Continuity equation:

$$\frac{\partial}{\partial t}(\alpha_i\rho_i) + \nabla\cdot(\alpha_i\rho_i\vec{v}_i) = S_i + \dot{m}_{ji} - \dot{m}_{ij} \qquad (1)$$

B. The momentum equation:

$$\frac{\partial(\alpha_i\rho_i\vec{v}_i)}{\partial t} + \nabla\cdot(\alpha_i\rho_i\vec{v}_i\vec{v}_i) = -\alpha_i\nabla p + \nabla\cdot\bar{\bar{\tau}}_i + \alpha_i\rho_i\vec{g} + \dot{m}_{ji}\vec{v}_j - \dot{m}_{ij}\vec{v}_i + \vec{F}_{D,i} + \vec{F}_{L,i} + \vec{F}_{wl,i} + \vec{F}_{td,i} + \vec{F}_{vm,i} \qquad (2)$$

C. The energy equation:

$$\frac{\partial}{\partial t}(\alpha_i\rho_i h_i) + \nabla\cdot(\alpha_i\rho_i\vec{v}_i h_i) = \alpha_i\frac{\partial p_i}{\partial t} - \nabla\cdot\vec{q}_i + S_i + Q_{ij} + \dot{m}_{ji}h_j - \dot{m}_{ij}h_i \qquad (3)$$

In the Eqs. (1) to (3), ρ_i,α_i, $\vec{v_i}$, S_i, P_i, $\bar{\bar{\tau}}_i$, $\vec{q}_i$ and h_i express the density, volume fraction, velocity, source term, pressure, stress tensor, heat flux, and specific enthalpy for the associated phase (ith phase), respectively.

D. CHF model

The Here, the RPI boiling model used to calculate CHF follows,

$$q_w = f(\alpha_f)\left(q_c + q_e + q_q\right) + \left(1 - f(\alpha_f)\right)q_g \qquad (4)$$

where q_w is the total heat flux, transferred to the fluid from the heated wall. The total heat flux has two components; one is the liquid phase heat flux (q_f) and the other is the vapor phase heat flux (q_g). The liquid heat flux consists of three parts: q_c, q_e and q_q, which are the single-phase convective heat flux, the evaporate heat flux and the wall quenching heat flux, respectively.

In the E(4), the fraction of the wall area heated by the liquid phase is $f(\alpha_f)$ and the fraction of heated wall area dominated by single-phase vapor is defined by $\left(1 - f(\alpha_f)\right)$. the Loilev *et al.* model has been used here for evaluation of $f(\alpha_f)$[13],

$$f(\alpha_f) = 1 - \max\left(0, \min\left\{1, \frac{\alpha_g - \alpha_{g,1}}{\alpha_{g,2} - \alpha_{g,1}}\right\}\right) \qquad (5)$$

To the calculate the four heat fluxes, four relationships are used,

$$q_C = h_f(T_w - T_l)(1 - A_b) \qquad (6)$$

$$q_e = V_d N_w \rho_g h_{fg} f \qquad (7)$$

$$q_q = \frac{2\sqrt{k_l\rho_l C_{P,l} f}}{\sqrt{\pi}}(T_w - T_l) \qquad (8)$$

$$q_g = h_g\left(T_w - T_g\right) \qquad (9)$$

where h_f and h_g, are the single-phase heat transfer coefficient for liquid and vapor phase, respectively. In the (6-9), T_l, T_w, and T_g represent the temperature of liquid, heated wall and vapor phase, correspondingly; ρ_l is the density of the liquid phase and ρ_g , the density of vapor phase. In (7), h_{fg} and V_d are defined as latent heat of evaporation and the volume of the bubbles, accordingly. In (6), $(1 - A_b)$ and A_b, appeared in (10), are the proportion of heated wall covered by nucleating bubbles and single-phase liquid respectively.

$$A_{\mathrm{b}} = \min\left(1, K\frac{N_{\mathrm{w}}\pi d_{\mathrm{Bw}}^2}{4}\right) \quad (10)$$

in which d_{bw}, denotes the bubble departure diameter. The model of Tolubinsky and Kostanchuk is adopted for the purpose of calculation of the bubble departure diameter [14]:

$$d_{BW} = MIN\left(1.4\ [mm], 0.6\ [mm].\exp\left(-\frac{\Delta T_{sub}}{45\ [k]}\right)\right) \quad (11)$$

In (10), K and N_{w} are empirical constant and active nucleate site density, respectively. To estimate the empirical constant (K), *t* Del Valle and Kenning equation has been used[15].

$$\mathrm{K} = 4.8\exp\left(-\frac{\rho_l C_{P,l}(T_w - T_l)}{80\rho_g h_{fg}}\right) \quad (12)$$

To calculate the active nucleate site density (N_{w}), also, the model of Lemmert and Chawla was used [16].

$$N_{\mathrm{w}} = [210(T_w - T_{sat})]^{1.805} \quad (13)$$

IV. Geometry and boundary conditions

Evaluation The geometry is a stainless steel tube, and with the diameter and total length considered to be 2.56 mm and 200 mm, respectively. The length of the tube is divided into two halves. The second half of the tube has been heated, while the first half has been not. Liquid mass flux, relative pressure and constant heat flux are considered for tube inlet, tube outlet, and tube wall, respectively. No slip boundary conditions are applied on the tube wall. The value of the fluid properties varies according to the fluid pressure and temperature. A coupled algorithm has been used to solve equations of the problem. CFD's calculations are carried out by the commercial code FLUENT 17.2, ANSYS Inc. In order to obtain CHF values as seen in the experimental researches, the heat flux increases by small steps until the amount of the surface temperature increases suddenly. In this study, the amount of the heat flux is about 80 % of the critical heat flux as compared with the experimental studies. After the results convergence, the heat flux value increases with the steps of 100 kW/m^2 and the simulations are repeated until the wall temperature experiences a sudden increase, where the heat flux is called the critical heat flux.

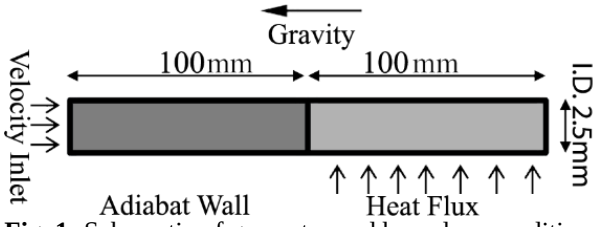

Fig. 1: Schematic of geometry and boundary conditions.

V. Validation and Results

The variations of the wall temperature versus the length of the tube for G=30 Kg/m^{2}s and P=800 *kPa* has been shown in fig. 2. As it can be seen, since the heat flux is not applied to the first half of the tube, the wall temperature for first half is constant along the tube length, while as the constant heat flux is applied to the second half of the tube, the wall temperature of the tube is steadily increasing. As shown in fig. 2, in the heat flux value of 38.7 MW/m^2, the variation of the temperature at the end of the second half of the tube is very sever, that is, we have a critical heat flux value at this point for the present condition.

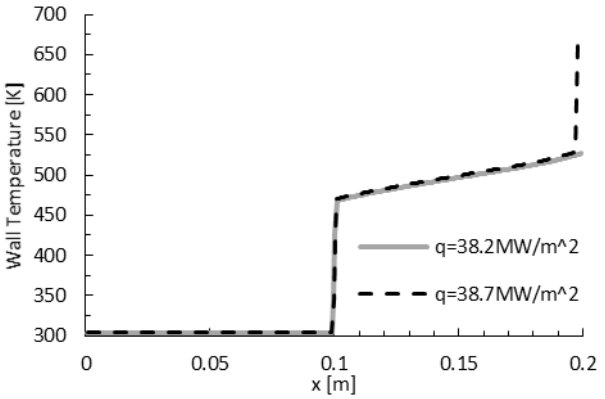

Fig. 2: Variation of tube wall temperature at q=38.2MW/m^2 and CHF (q=38.7MW/m^2)

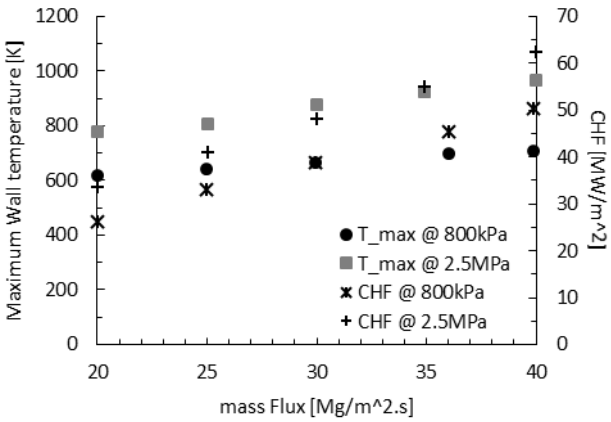

Fig. 3: Maximum tube wall temperature at CHF.

As shown in fig. 3, the maximum temperature is dependent on the working conditions of the fluid. Therefore, it can be concluded that for some working conditions, if the appropriate material is used for the tube, the CHF would not be risky.

The result of the simulation for inlet temperature about 30°C and two different pressures of 800 *kPa* and 2.5 *MPa* are shown in figs. 4-5. In the case of fig. 5, two experiments have been carried out for two different inlet mass fluxes of 30000 Kg/m^{2}s and 40000 Kg/m^{2}s, respectively, where each of the experiments has different CHF values [12]. The results in figs. 4-5 show good validity between the present study and the research by Celata *et al.* [12]. The Mean Absolute Error (MAE) for scenarios of figs. 4-5, is about 3% and 9.4 %, respectively. For a more accurate comparison, the results of figs. 4-5 are shown by error guidance lines of 15 % in fig. 6.

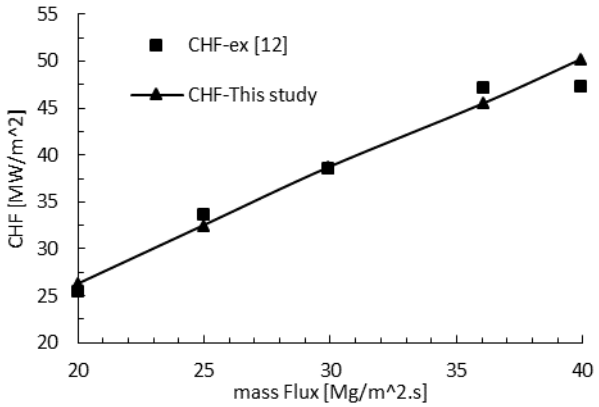

Fig. 4: CHF variations versus the mass flux (T_{in}=30°C, P=800 *kPa*)

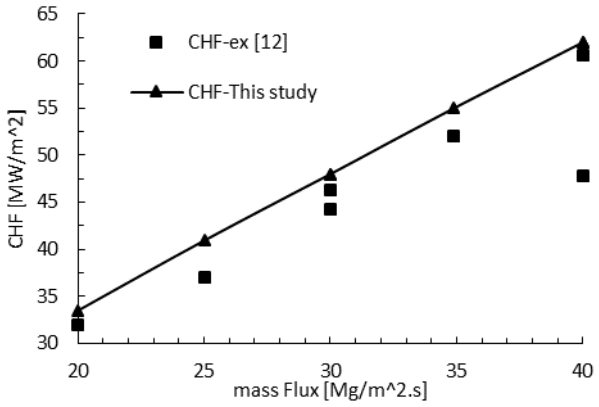

Fig. 5: CHF variations versus the mass flux (T_{in}=30°C, P=2.5 *MPa*)

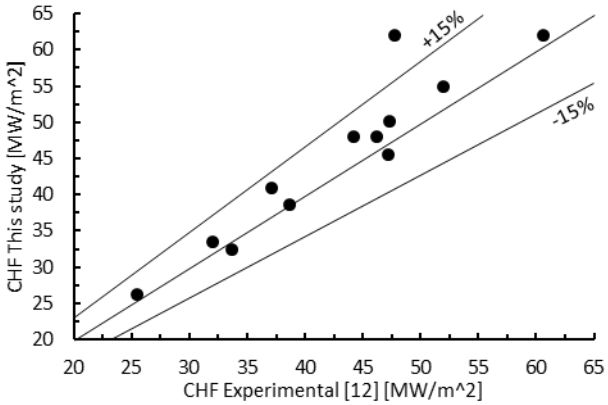

Fig. 6: A comparison between the experimental and simulated CHF (T_{in}=30°C, P=800 *kPa* and P=2.5 *MPa*)

The result of experimental and simulated CHF in terms of the inlet fluid temperature is shown in figs. 7 and 8. The results are for two different inlet mass fluxes (20000 Kg/m^{2}s, 30000 Kg/m^{2}s) and a working pressure of about 800 *kPa*. Observation of these figures demonstrates that CHF value decreases as the inlet flow temperature increases. Also, the corresponding MAEs are about 8.9% and 4 %, respectively.

For a more accurate examination of the results pictured in figs. 7 and 8, all the data are shown in fig. 9 by taking a guideline of 15 % into consideration. The MAE for fig. 9 is about 6.5 %. All the results presented in figs. 6 and 9 are shown with error guidelines of 15 % in fig. 10. This figure consists of 22 resulted of both the experimental and simulated studies. As shown here, the amount of error for the results, in most conditions, is less than 10 %, which is an acceptable performance for simulation. The MAE of the simulations is about 6.7 %.

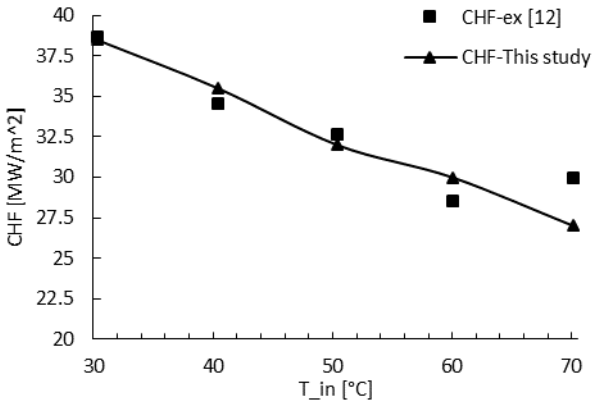

Fig. 7: CHF variations versus the mass flux (G=20Mg/m^{2}s and P=800 *kPa*).

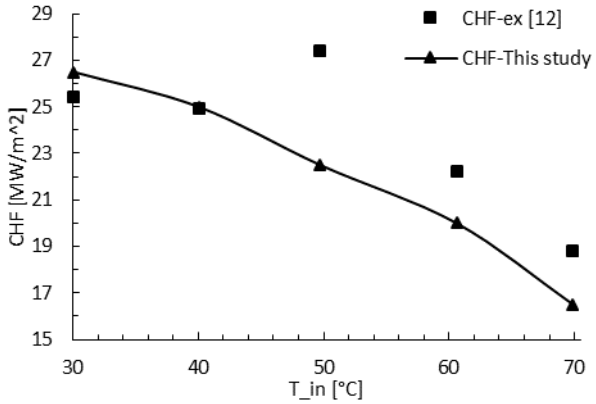

Fig. 8: CHF variations versus the mass flux (G=20Mg/m^{2}s and P=800 *kPa*).

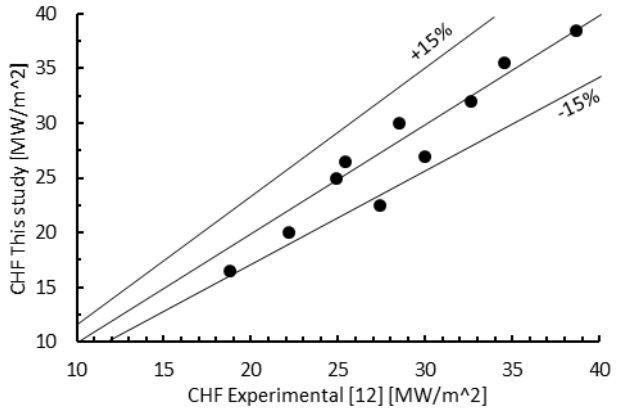

Fig. 9: Comparison between the experimental and simulated CHF (P=800 *kPa*, G=20Mg/m^{2}s and G=30Mg/m^{2}s).

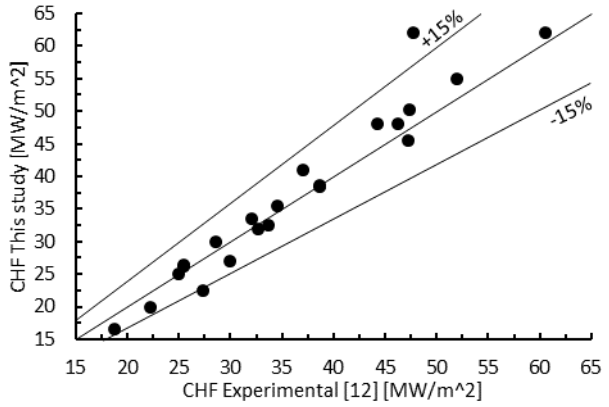

Fig. 10: comparison between the experimental and simulated CHF for all results.

As discussed in the previous sections, the tube has a total length of 200 mm, of which only the second half is under constant heat flux. Thus, the first half of the tube has been omitted for further studies and simulations. As shown in fig. 11, simulations are carried out for inlet fluid flow with temperature 30 ° C and two different pressures of 800 *kPa* and 2.5 *MPa*. From the fig. 11, the CHF value for the tube with length of 100 mm is less than the tube with length of 200 mm. The MAEs for tube with lengths 200 mm and 100 mm, are about 7.8 % and 5.7 %, respectively.

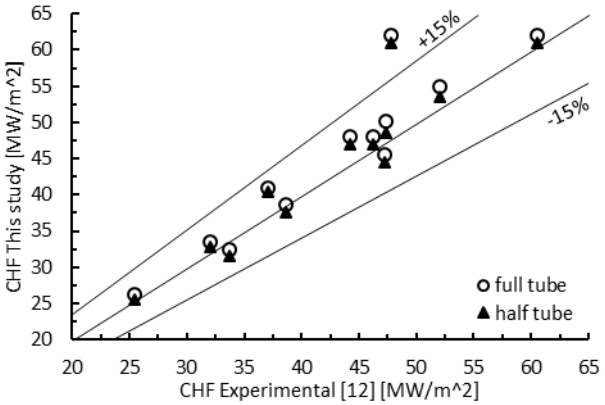

Fig. 11: CHF comparison for 200mm and 100mm tube.

VI. Conclusion

In this paper, two phase flow of water liquid and water vapor has been investigated. The aim of this study is to investigate the CHF phenomenon caused by flow boiling inside the vertical tube. The results of this study are compared with experimental data, which demonstrated the error of simulations is less than 7 %. The maximum wall temperature value in the onset of CHF is variable for different conditions. This parameter as well as the CHF value increase as the pressure and mass flux increase. During the experiments, a part of the tube was considered without the applying the heat flux. In the simulations, two cases have been investigated. In the first scenario, a tube with length of 100 mm was considered, where all the tube was under the constant heat flux, while in the second scenario, a tube of the length 200 mm was assumed, such that only the second half pf the tube was under the constant heat flux. It has been observed that the CHF value for the tube with length of 100 mm is less than the tube with length of 200 mm.

References

[1] Kim, S.J., McKrell, T., Buongiorno, J. and Hu, L.W., 2009. Experimental study of flow critical heat flux in alumina-water, zinc-oxide-water, and diamond-water nanofluids. Journal of Heat Transfer, 131(4), p.043204.

[2] Chen, E., Li, Y. and Cheng, X., 2009. CFD simulation of upward subcooled boiling flow of refrigerant-113 using the two-fluid model. Applied Thermal Engineering, 29(11-12), pp.2508-2517.

[3] Ose, Y. and Kunugi, T., 2011. Development of a boiling and condensation model on subcooled boiling phenomena. Energy Procedia, 9, pp.605-618.

[4] Krepper, E. and Rzehak, R., 2011. CFD for subcooled flow boiling: Simulation of DEBORA experiments. Nuclear Engineering and Design, 241(9), pp.3851-3866.

[5] Krepper, E., Končar, B. and Egorov, Y., 2007. CFD modelling of subcooled boiling—concept, validation and application to fuel assembly design. Nuclear Engineering and Design, 237(7), pp.716-731.

[6] Krepper, E., Rzehak, R., Lifante, C. and Frank, T., 2013. CFD for subcooled flow boiling: Coupling wall boiling and population balance models. Nuclear engineering and design, 255, pp.330-346.

[7] Kurul, N., 1991. On the modeling of multidimensional effects in boiling channels. ANS. Proc. National Heat Transfer Con. Minneapolis, Minnesota, USA, 1991.

[8] Nasiri, M. and Mahdi Rashidi, M., 2015. Numerical study of Subcooled Flow boiling of Water-Al 2 O 3 in vertical sinusoidal wavy channel. Modares Mechanical Engineering, 14(11).

[9] Alimoradi, H., Shams, M. and Valizadeh, Z., 2017. The effects of nanoparticles in the subcooled boiling flow in the channels with different cross-sectional area and same hydraulic diameter. Modares Mechanical Engineering, 16(12), pp.545-554.

[10] M. Mohammadi, M. Khayat, Experimental investigation of the effect of roughness orientation of surface on motion of bubbles and critical heat flux, Modares Mechanical Engineering, Vol. 17, No. 12, pp. 531-541, 2018.

[11] Wang, Y., Deng, K., Wu, J., Su, G. and Qiu, S., 2018. The characteristics and correlation of nanofluid flow boiling critical heat flux. International Journal of Heat and Mass Transfer, 122, pp.212-221.

[12] G. Celata, M. Cumo, A. Mariani, Burnout in highly subcooled water flow boiling in small diameter tubes, International Journal of Heat and Mass Transfer, vol. 36, pp. 1269-1285, 1993.

[13] Ioilev, A., Samigulin, M., Ustinenko, V., Kucherova, P., Tentner, A., Lo, S. and Splawski, A., 2007, September. Advances in the modeling of cladding heat transfer and critical heat flux in boiling water reactor fuel assemblies. In Proc. 12th International Topical Meeting on Nuclear Reactor Thermal Hydraulics (NURETH-12), Pittsburgh, Pennsylvania, USA.

[14] Tolubinsky, V.I. and Kostanchuk, D.M., 1970. Vapour bubbles growth rate and heat transfer intensity at subcooled water boiling. In International Heat Transfer Conference 4 (Vol. 23). Begel House Inc.

[15] Del Valle, V.H. and Kenning, D.B.R., 1985. Subcooled flow boiling at high heat flux. International Journal of Heat and Mass Transfer, 28(10), pp.1907-1920.

[16] Lemmert, M. and Chawla, L.M., 1977. Influence of flow velocity on surface boiling heat transfer coefficient in Heat Transfer in Boiling. Academic Press and Hemisphere, New York, NY, USA.

Appendix

Nomenclature	
d_{bw}	Bubble departure diameter
G	Mass flux
$\vec{q}_w$	Total heat flux
q_c	Single-phase convective heat flux
q_e	The evaporate heat flux
q_q	Quenching heat flux
N_w	Nucleate site density
V_{d}	Bubble volume
f	Bubble departure frequency
c_p	Specific heat at constant pressure
h_{fg}	Latent of vaporization
S	Heat source
h	Heat transfer coefficient
Greek symbols	
α	Void fraction
ρ	Density
$\bar{\bar{\tau}}_\iota$	Stress tensor
Subscripts	
g	Gas
l	Liquid
i	i phase
j	j phase
sat	Saturation
w	Wall
Sub	Subcooled fluid